Electroproduction of Pions from Hydrogen and Deuterium*

GERALD G. OHLSEN†
Department of Physics and High-Energy Physics Laboratory, Stanford University, Stanford, California
(Received June 6, 1960)

The absolute cross section for direct production of pions in electron-proton and in electron-deuteron collisions has been measured by the detection of inelastically scattered electrons. Proton data have been taken throughout the range of $q^2=2.6$ f^{-2} to $q^2=10.75$ f^{-2}, and center-of-mass energy $E=1100$ Mev to $E=1300$ Mev. Data analysis has been in terms of a neutron magnetic moment distribution. Comparison with available theory yields a neutron rms magnetic moment of 1 f, but better theoretical calculations may change this value somewhat. No theory for the electroproduction of pions from deuterons exists at present. The deuteron data are presented in terms of absolute cross sections as well as in terms of a deuteron-proton cross-section ratio.

I. INTRODUCTION

PANOFSKY and Allton[1] have recently investigated the production of pions in electron-proton collisions in an attempt to obtain information about neutron electromagnetic structure. This experiment is an extension of their work to higher values of the 4-momentum transfer and over a wider range of center-of-mass energies. Also, the experiment was repeated using a deuteron target.

For a proton target, the reactions of interest may be written

$$e+p\rightarrow e'(\theta)+n+\pi^+, \tag{1}$$

$$e+p\rightarrow e'(\theta)+p+\pi^0. \tag{2}$$

In order to obtain information about nucleon structure, it is necessary to single out those events which correspond to a large 4-momentum transfer. Thus, since the initial and final electron energies together with the laboratory electron scattering angle completely determine the 4-momentum transfer as well as the energy delivered to the pion-nucleon system, observation of the inelastically scattered electrons is preferable to the observation of the pions. This procedure was therefore followed in both this experiment and the Panofsky-Allton experiment. Since only the final electron is observed, the sum of the cross sections for the reactions (1) and (2) is measured.

The connection between the invariant 4-momentum transfer q and the laboratory quantities may be written (neglecting the rest mass of the electron)

$$q^2=2E_1E_2(1-\cos\theta), \tag{3}$$

where E_1 and E_2 are the laboratory incident and final electron energies, respectively, and θ is the laboratory scattering angle. (We use, throughout, units in which $\hbar=c=1$.) The energy E of the pion and nucleon in their center-of-mass system (including rest energies) is related to the laboratory quantities by the relation

$$E^2=M^2+2M(E_1-E_2)-2E_1E_2(1-\cos\theta), \tag{4}$$

where M is the rest mass of the proton, and again the rest mass of the electron has been neglected. A large part of the data was taken at $E=1200$ Mev, which corresponds approximately to the energy at which the $(\frac{3}{2},\frac{3}{2})$ pion-nucleon resonance produces a maximum in the cross sections.

The angles used in this experiment were 90° and 135° (laboratory) while the incident electron energies ranged from 461 to 684 Mev. The scattered electron energy range of primary interest was from about 100 to 180 Mev.

The deuteron experiment was performed in an attempt to obtain information about the neutron reactions corresponding to (1) and (2), namely

$$e+n\rightarrow e'(\theta)+p+\pi^-, \tag{5}$$

$$e+n\rightarrow e'(\theta)+n+\pi^0, \tag{6}$$

although at the present time no theory exists which would enable one to extract such information from the measured deuteron cross section. The measured cross section corresponds to the reactions

$$e+d\rightarrow e'(\theta)+p+p+\pi^-, \tag{7}$$

$$e+d\rightarrow e'(\theta)+n+n+\pi^+, \tag{8}$$

$$e+d\rightarrow e'(\theta)+p+n+\pi^0, \tag{9}$$

$$e+d\rightarrow e'(\theta)+d+\pi^0. \tag{10}$$

II. THEORY

According to the analysis of Dalitz and Yennie,[2] the expression for the inelastic electron scattering cross section corresponding to any of reactions (1), (2), (5), or (6) may be written

$$\frac{d^2\sigma}{d\Omega dE_2}=\frac{\alpha}{32\pi^3}\frac{S}{E}\frac{E_2}{E_1}Mm^2[|\langle j_\mu\rangle A^\mu|^2]_{\text{av}}, \tag{11}$$

where α is the fine structure constant, S is the magnitude

* Supported by the Office of Naval Research, the U. S. Atomic Energy Commission, and the Air Force Office of Scientific Research.

† Now at the University of Texas, Austin, Texas.

[1] W. K. H. Panofsky and E. A. Allton, Phys. Rev. **110**, 1155 (1958).

[2] R. H. Dalitz and D. R. Yennie, Phys. Rev. **105**, 1598 (1957).

of the pion momentum in the center-of-mass system, m is the electron mass, $\langle j_\mu \rangle$ is the appropriate transition current matrix element to go from the initial nucleon to the final pion-nucleon state, and A^μ is the Møller potential of the scattered electron. Other quantities are as defined earlier. The quantity $|\langle j_\mu \rangle A^\mu|$ is averaged over final pion directions and appropriate spin sums are taken.

At the present time, the best available expressions for the matrix elements $\langle j_\mu \rangle$ are those obtained by Fubini, Nambu, and Wataghin,[3] who used a dispersion theoretical approach. An explicit dependence of these matrix elements on the nucleon form factors enables the proton data analysis to be in terms of nucleon structure. An important fact here is that the matrix element corresponding to each of the reactions (1), (2), (5), and (6) depends on the electromagnetic structure of both the proton and the neutron. Thus, since the proton structure is well known from other experiments,[4] the measured cross sections corresponding to reactions (1) and (2) may be interpreted in terms of a neutron structure. Reactions (5) and (6) are of course not directly observable.

Near the threshold for these processes (center-of-mass energy $E=1079$ Mev) the dependence of the theoretical cross sections on the neutron charge structure is large, while the dependence on the magnetic moment structure is small. However, near the pion-nucleon $(\frac{3}{2},\frac{3}{2})$ resonance (approximately $E=1200$ Mev) the situation is reversed. Since most of the data in this experiment were taken well above threshold, the neutron charge form factor has been assumed identically zero and the interpretation has been made in terms of its magnetic moment structure alone.

Gartenhaus and Lindner[5] have evaluated Eq. (11) using slight simplifications of the matrix elements of Fubini *et al.* In particular, they have neglected all longitudinal contributions to the cross section. The results of their calculation were used throughout this paper.

As stated above, no theory exists for the deuteron process. As a crude first estimate of the expected cross sections, the deuteron momentum distribution has been folded into the theoretical stationary proton and neutron cross sections. As will be seen later, the experimental cross sections are somewhat smaller than the result of this folding.

III. EXPERIMENTAL DETAILS

A diagram of the experimental arrangement is given in Fig. 1. The beam from the Stanford Mark III linear accelerator was energy-analyzed and focussed on a liquid hydrogen (or liquid deuterium) target. The beam was monitored with a secondary emission monitor,[6] which was periodically calibrated against a large Faraday cup. The Faraday cup was removed from the beam during the actual cross-section measurements, since its presence causes a large flux of neutrons to impinge on the counter system, and thus creates a large background.

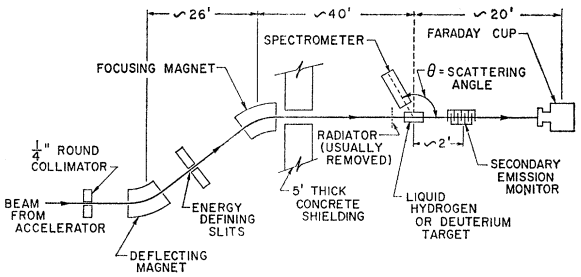

FIG. 1. Diagram of experimental arrangement.

The inelastically scattered electrons were energy-analyzed using a 36-in. radius 180° magnetic spectrometer which has been described elsewhere,[7] and counted with a two-element Čerenkov counter coincidence system. The front counter was a $\frac{7}{8}$-in. thick Lucite block viewed from one edge by an RCA-6810-A photomultiplier tube. The rear counter was in the shape of a truncated cone, viewed from the larger end by an RCA-7046 photomultiplier tube. The output of the two counters was fed into a fast coincidence circuit of the type designed by Wenzel.[8] The variation of counting efficiency with energy was measured by the comparison of measured elastic hydrogen counting rates to the known cross sections at various scattered electron energies. The efficiency of the counting system was found to be energy independent over the range of interest, i.e., from 100 to 180 Mev.

IV. REMOVAL OF COMPETING PROCESSES

Several processes contribute low-energy (100–180 Mev) electrons in addition to the electropion processes which are of interest here. Panofsky and Allton[1] have devised an extrapolation procedure to remove the undesired events. With minor modifications, their method is used here.

There are three general ways other than through the electropion processes through which a significant number of low-energy electrons arise: (1) An incident electron may emit a large photon before, after, or during nuclear scattering into the direction of observation. (The first two of these processes are thick-target effects, while the last process is known as wide-angle bremsstrahlung.) (2) Photons produced in the target (or the virtual photons of the electron's electromagnetic field)

[3] S. Fubini, Y. Nambu, and V. Wataghin, Phys. Rev. **111**, 329 (1958).
[4] R. Hofstadter, F. Bumiller, and M. R. Yearian, Revs. Modern Phys. **30**, 482 (1958).
[5] S. Gartenhaus and C. N. Lindner, Phys. Rev. **113**, 917 (1959).
[6] G. W. Tautfest and H. R. Fechter, Rev. Sci. Instr. **26**, 229 (1955).
[7] R. Hofstadter, Revs. Modern Phys. **28**, 214 (1956).
[8] W. A. Wenzel, University of California Radiation Laboratory Report UCRL-8000 (unpublished).

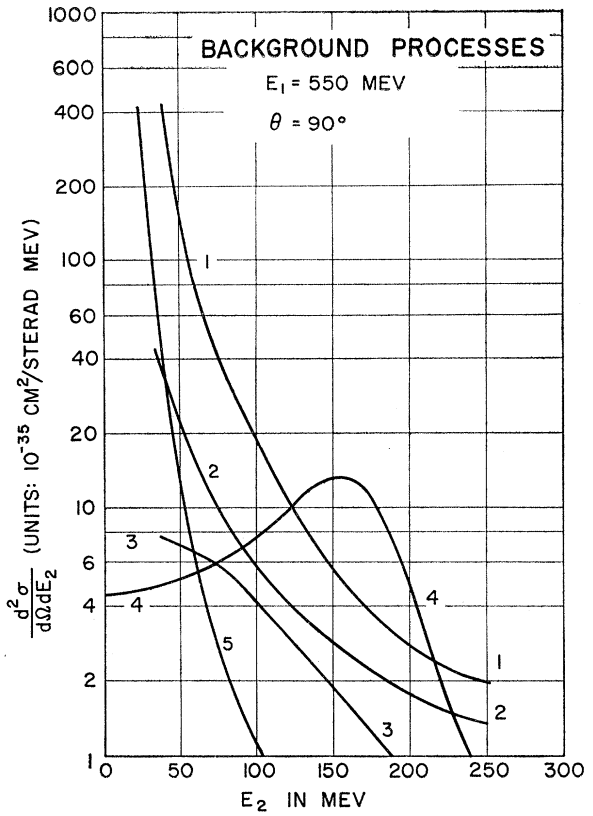

FIG. 2. Comparison of observed and calculated background contributions to the electropion cross section for the case $E_1=550$ Mev, $\theta=90°$: (1) observed sum of competing processes (experimental cross section for all processes decreased by the theoretical electropion cross section), (2) theoretical contributions due to bremsstrahlung, (3) approximate contribution due to charged and neutral pions, (4) theoretical electropion cross section (assuming the rms neutron magnetic moment radius to be 1.0 f), and (5) approximate contributions from electron-electron scattering followed by elastic nuclear scattering.

may produce π^0 or π^- mesons. The π^0 decay photons may then give rise to electron-positron pairs, or pairs may be emitted directly via Dalitz decay. The π^- mesons may give rise to electrons through the π-μ-e decay. (3) Electron-electron scattering may produce a large number of low-energy electrons. These electrons, which will be sharply peaked in the forward direction, may then suffer elastic nuclear scattering into the direction of observation. Contributions from many other processes have been considered and found to be negligible for the experimental conditions used here. For a particular case, the relative contributions from the processes listed above are shown in Fig. 2.

The first two effects may be removed by an extrapolation procedure, which will be described in detail, while the contributions from the third process becomes very small, and will therefore be neglected, at energies above 100 Mev. On the other hand, contributions from the third process become very large for sufficiently low electron energies, and thus set a lower limit to the experimentally accessible scattered electron energy range. An experimental upper limit to the accessible energy range is set by the π-meson Čerenkov threshold, which, for the counting system used here, corresponds to a momentum of $\sim$180 Mev/c. Thus we are restricted to the narrow scattered-electron energy band between about 100 and 180 Mev. This proves not to be a serious constraint.

For the case of a hydrogen target, it can be shown[1] that the contributions from the first two processes can be approximately removed by inserting a "radiator" ahead of the target, measuring the increase in counting rate, and linearly extrapolating to zero radiator thickness via the expression

$$C=C_0-\frac{t_1[kN(k)]+N_B}{t_R[kN(k)]}(C_R-C_0), \tag{12}$$

where C_R and C_0 are the counting rates with and without radiator, respectively, and C is the extrapolated counting rate. The quantity t_1 is the effective thickness of the target in radiation lengths, t_R is the thickness of the radiator in radiation lengths, N_B is the equivalent radiation length for wide-angle bremsstrahlung, k is the relevant photon energy ($k=E_1-E_2$), and $N(k)$ is the photon spectrum which would be produced by 1 radiation length of the relevant material, as computed from the Bethe-Heitler formula.[9] [Thus $kN(k)$ is a bremsstrahlung spectrum shape correction factor of order unity.] N_B is given by[1]

$$N_B=\frac{\alpha}{\pi}\left[1+\left(\frac{E_2}{E_1}\right)^2\right]\left[\ln\left(\frac{2E_1}{m}\sin(\theta/2)\right)-\tfrac{1}{2}\right], \tag{13}$$

where m is the electron mass, θ is the laboratory angle of observation, and α is the fine structure constant.

We have used a slightly modified form in which no terms have been dropped as was done in the derivation of Eq. (12), namely,

$$C=C_0-\epsilon(C_R-C_0), \tag{14}$$

where $\epsilon=(N_{\text{target}}+N_B)/N_{\text{radiator}}$, with

$$N_{\text{target}}=\frac{t_1[k\,N(k)_{\text{target}}]\frac{d\sigma}{d\Omega}(E_2)+t_2[k\,N(k)_{\text{target}}]\frac{d\sigma}{d\Omega}(E_1)}{\frac{d\sigma}{d\Omega}(E_2)+\frac{d\sigma}{d\Omega}(E_1)},$$

and

$$N_{\text{radiator}}=\frac{t_R[k\,N(k)_{\text{radiator}}]\frac{d\sigma}{d\Omega}(E_2)}{\frac{d\sigma}{d\Omega}(E_2)+\frac{d\sigma}{d\Omega}(E_1)},$$

[9] H. A. Bethe and J. Ashkin, in *Experimental Nuclear Physics*, edited by E. Segrè (John Wiley & Sons, Inc., New York, 1953), Vol. I, pp. 259 ff.

where the $N(k)$ appropriate to the target and radiator materials is used. The quantities t_1 and t_2 are the thicknesses of target (in radiation lengths) penetrated before and after the elastic scattering event, respectively, and $d\sigma/d\Omega(E_1)$ and $d\sigma/d\Omega(E_2)$ are the elastic electron-proton cross sections evaluated at the appropriate angle and at incident electron energies of E_1 and E_2, respectively.

Numerically, the values of t_1 and t_2 were about 0.0130 and 0.0050 radiation lengths, respectively. N_B is of the order of 0.015, although it varies with energy. The thickness of the copper radiators used for the extrapolation were 0.0345 radiation lengths (0.442 g/cm^2; referred to hereafter as "thick" radiator) and 0.0173 radiation lengths (0.221 g/cm^2; referred to hereafter as "thin" radiator). Most of the radiator data were taken using the thick radiator.

As mentioned above, the third process makes a significant contribution only for scattered electron energies less than about 100 Mev. An expression for the contribution from this source may be written[10]

$$\frac{d^2\sigma}{d\Omega dE_2}=C\frac{Z}{A}\left[\frac{E_1}{E_2(E_1-E_2)}-\frac{1}{E_1}\right]^2\frac{d\sigma}{d\Omega}(E_2), \quad (15)$$

where C is 0.0153 times the target thickness in g/cm^2, Z and A are the atomic number and the atomic mass number, respectively, for the target material, and other quantities are as defined above. This expression varies approximately as $(E_2)^{-4}$ and becomes negligible in the energy region of interest.

All formulas stated in this section neglect the recoil of the target proton in the elastic scattering. However, since ϵ, the quantity of interest, involves a ratio of quantities each of which is based on this assumption, this should not introduce a significant error into the extrapolation.

As a check on the extrapolation procedure, the spectrometer current was occasionally reversed and positive-particle counting rates with and without the radiator were observed. If the extrapolation procedure is valid, it should yield a null result in each case. Within the statistical error of the measurement, this was found to be the case.

The same procedure was used to extrapolate the deuteron data, although it cannot be as well justified in this case. However, by a general Weizsäcker-Williams type argument, the procedure should remain approximately correct.

V. NORMALIZATION OF DATA

Absolute cross sections were obtained through comparison to proton elastic scattering data, taken with the same experimental arrangement, in conjunction with the well-known[4] elastic cross section. The energy of the elastic peak was always chosen to fall near the center of the energy range covered by the inelastic spectrum of interest. Specifically, taking into account the constant fractional momentum acceptance of the spectrometer, the counting rate at a given energy of the inelastic spectrum can be converted to an absolute cross section by the following relation:

$$\frac{d^2\sigma}{d\Omega dE_2}=\left[\frac{\frac{d\sigma}{d\Omega}(E_1)}{\int_{E_0-\Delta E}^{E_{\max}}\frac{C_{\text{elastic}}(E)}{E}dE}\exp(-\delta_B-\delta_R)\right]\times\frac{C(E_2)}{E_2}, \quad (16)$$

where E_1 is the primary beam energy used for the normalization, $d\sigma/d\Omega(E_1)$ is the calculated elastic Rosenbluth cross section using an exponential model[4] with charge and magnetic moment radius 0.8 f, E is the energy of elastically scattered electrons, E_0 is the energy at the peak of the elastic spectrum, $E_{\max}$ is some energy sufficiently greater than E_0 for the elastic counting rate to be zero, E_2 is the inelastic energy of interest, $C_{\text{elastic}}(E)$ is the number of elastic counts at energy E, and $C(E_2)$ is the number of inelastic counts at energy E_2, where this last quantity is to be obtained from the raw data by using Eq. (14). $C_{\text{elastic}}(E)$ and $C(E_2)$ must of course be normalized to the same integrated beam current. For the deuteron inelastic data, an additional factor must be included to take into account the difference of atomic densities in liquid hydrogen and liquid deuterium. The quantity $\exp(-\delta_B)$ is the usual bremsstrahlung correction, where

$$\delta_B=\frac{t_1+t_2}{\ln(2)}\ln\left(\frac{E_0}{\Delta E}\right), \quad (17)$$

with t_1+t_2 the effective target radiation length; $\exp(-\delta_R)$ is the Schwinger correction,[11] where

$$\delta_R=\frac{4\alpha}{\pi}\left\{\left[\ln\left(\frac{E_0}{\Delta E}\right)-\frac{13}{12}\right]\times\left[\ln\left(\frac{2E_0\sin(\theta/2)}{m}\right)-\frac{1}{2}\right]+\frac{17}{72}\right\}. \quad (18)$$

The quantity ΔE is the instrumental resolution, or, in practice, the difference between the peak energy E_0 and the lowest energy to which the elastic curve is extended. In this case, ΔE was taken as twice the full width of the elastic peak at half-maximum.

In practice, the variation of the beam monitor efficiency must be carefully measured, since the usual

[10] B. Rossi, *High-Energy Particles* (Prentice Hall, Inc., New York, 1952), pp. 14 ff.

[11] R. Hofstadter, Revs. Modern Phys. **28**, 214 (1956). Hofstadter's Eq. (31) contains two misprints which have been corrected here.

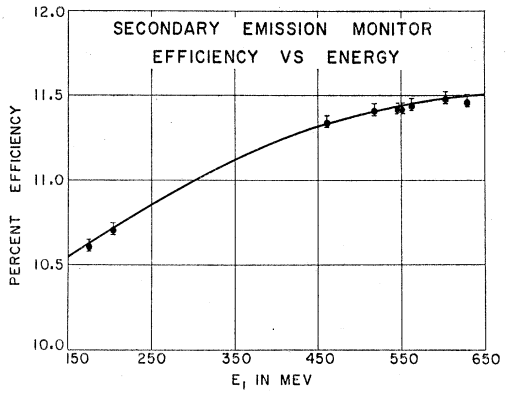

FIG. 3. Secondary emission monitor efficiency plotted versus electron energy.

primary energies for normalizations were around 200 Mev, while the energies used for the electropion production were around 600 Mev. The variation of efficiency with energy for the secondary emission monitor used in the later runs is shown in Fig. 3.

Random background was frequently measured either by removing the target and replacing it with a radiator of about the same thickness, but out of view of the spectrometer, or by setting the spectrometer current so high that no energetically possible particles could be transmitted through it. In no case did this type of background exceed 2% of the total counting rate, and in most cases it was considerably less important.

VI. ERRORS

The extrapolation factor ϵ is computed from a ratio of similarly derived quantities, each of which is thought to be correct to within 10%. Since the errors in the numerator and denominator are presumably in the same direction, they tend to cancel. Thus, ϵ is thought to be accurate to about 5%. This uncertainty is allowed for in the larger of the error estimates presented with the data. Near $E=1200$ Mev, where electropion processes contribute 60–70% of the raw counting rate, this uncertainty should lead to no more than a 2% error in the final cross section.

Elastic normalizations were carried out with a statistical accuracy of about 1%. Radiative corrections to the elastic data introduce a possible error of the order of 2%. Monitor efficiency fluctuations may introduce an error as large as 2%. Uncertainty in the counting-rate correction due to the fluctuations in the number of electrons in consecutive beam pulses may introduce a 1% error.

Another source of error is the uncertainty of the primary beam energy used for the normalization. Since the elastic cross section is approximately proportional to $(E_1)^{-2}$, the relative error $\Delta(d\sigma/d\Omega)(E_1)/(d\sigma/d\Omega)(E_1)$ is given by $2\Delta E_1/E_1$, where $\Delta E_1/E_1$ is the relative error in the calibration of the beam energy defining magnet. This calibration is known to about $\frac{1}{2}$%, and thus leads to an error of about 1%. Also, even at the low energies used here, the uncertainty in the proton size introduces an error perhaps as large as several percent.[4]

Combining all of the normalization errors listed above quadratically, a reasonable estimate of the total error is ~7%. This is to be compared with typical statistical errors on the inelastic data (after extrapolation) of 6 to 8%. Thus, the over-all accuracy of the experiment may be taken as about 10%.

VII. PROTON DATA

The proton data are summarized in Tables I and II. The quantities in the tables are as follows: E_1 is the initial electron energy; E_2 is the final electron energy; and E is the energy in the pion-nucleon center-of-mass system (including rest masses). The quantity q^2 is the square of the 4-momentum transfer (in units of 10^4 Mev^2 and also in units of 10^{26} cm^{-2}). ϵ is the thick-radiator extrapolation factor. (The thin-radiator extrapolation factor is exactly twice the thick-radiator value.) The quantity σ_{thick} is the final extrapolated cross section using the thick-radiator data, and may be considered to be the final result of the experiment. The errors are statistical. The quantity $\Delta\sigma_{\text{thick}}{}^{\max}$ is the error of σ_{thick} when a 5% extrapolation factor uncertainty is included in addition to the statistical error. (This quantity corresponds to the outer error bars shown in Figs. 4–6.) The quantity σ_{thin} is the final extrapolated cross section using the thin radiator data; this may also be considered to be the final result of the experiment, but the errors are relatively large. The quantity $\Delta\sigma_{\text{thin}}{}^{\max}$ is the error of σ_{thin} when a 5% extrapolation factor uncertainty is included in addition to the statistical error. The quantity σ_{uncorr} is the cross section which results from the raw data with no subtractions whatever. The quantity $\sigma_{\max}$ is the uncorrected cross section σ_{uncorr} reduced by the calculated bremsstrahlung contribution. This may be considered to be an upper limit to the cross section since it neglects the remaining competing processes. The quantity $\sigma_{\text{uncorr}}{}^{+}$ is the cross section which results from the raw positive-particle data with no corrections whatever. The quantity $\sigma_{\text{thick}}{}^{+}$ is the extrapolated positive-particle cross section using thick-radiator data.

The quantities $\Delta\sigma_{\text{thick}}{}^{\max}$ and $\Delta\sigma_{\text{thin}}{}^{\max}$, as stated above, are the computed standard errors when a 5% uncertainty of the extrapolation factor is taken into account. It may be seen from the data that at the lower values of E_2 where the signal-to-background ratio is unfavorable, this uncertainty in the extrapolation factor becomes relatively important.

The results for $E_1=550$ Mev, $\theta=90°$ are plotted in Fig. 4, where the solid curves are the theoretical values predicted for various assumed values of the neutron magnetic moment radius r_{nm} (in fermis), according to the Gartenhaus-Lindner calculation.[5] The neutron magnetic form factor was computed using an exponential

TABLE I. Hydrogen electroproduction cross sections, laboratory angle 90°. (All cross sections in units of 10^{-35} cm²/sr Mev.)

E_1	E_2	E	q^2 (10^4 Mev²)	q^2 (10^{26} cm^{-2})	ϵ	σ_{thick}	$\Delta\sigma_{\text{thick}}^{\max}$	σ_{thin}	$\Delta\sigma_{\text{thin}}^{\max}$	σ_{uncorr}	$\sigma_{\max}$	$\sigma_{\text{uncorr}}^{+}$	$\sigma_{\text{thick}}^{+}$
461	109	1201	10.0	2.60	0.938	20.4 ±2.0	2.7			36.6 ±1.1	30.4 ±1.1		
523	225	1098	23.5	6.09	1.047	0.89±0.54	0.65			3.71±0.27	2.00±0.27		
	193	1140	20.2	5.23	1.006	5.81±0.77	0.87			8.42±0.42	6.32±0.42	10.5 ±0.8	2.90±1.59
	169	1170	17.7	4.57	0.985	9.79±1.00	1.12			13.2 ±0.6	10.7 ±0.6		
	146	1198	15.3	3.96	0.960	17.4 ±1.3	1.5	20.6 ±2.2	2.2	22.0 ±0.8	18.8 ±0.8	3.30±0.57	−1.66±1.19
	122	1227	12.8	3.31	0.939	19.1 ±1.7	2.1			28.2 ±0.9	23.8 ±0.9		
	96	1258	10.0	2.60	0.925	18.5 ±2.1	2.9			35.5 ±1.2	28.9 ±1.2	12.0 ±1.3	−0.04±2.56
550	248	1084	27.3	7.07	1.056	0.35±0.33	0.43			2.63±0.16	1.28±0.16		
	226	1114	24.9	6.44	1.035	1.46±0.33	0.43			3.81±0.17	2.30±0.17		
	206	1140	22.7	5.87	1.011	3.76±0.41	0.50			6.14±0.22	4.43±0.22		
	182	1171	20.0	5.19	0.985	8.71±0.57	0.67	9.81±1.34	1.35	11.3 ±0.3	9.24±0.30		
	170	1186	18.7	4.84	0.979	10.8 ±0.7	0.8			14.7 ±0.4	12.4 ±0.4		
	159	1200	17.5	4.53	0.968	13.2 ±0.8	0.9	12.8 ±1.2	1.3	17.4 ±0.4	14.8 ±0.4		
	154	1206	16.9	4.39	0.962	13.1 ±0.8	1.0			18.0 ±0.4	15.3 ±0.4		
	148	1214	16.3	4.22	0.956	16.1 ±0.8	1.0			20.6 ±0.5	17.7 ±0.5		
	144	1219	15.8	4.10	0.953	12.3 ±0.8	1.1			19.4 ±0.5	16.4 ±0.5		
	137	1227	15.1	3.90	0.951	12.6 ±0.9	1.2			20.3 ±0.5	16.9 ±0.5		
	113	1256	12.4	3.22	0.934	9.71±1.05	1.65			22.9 ±0.6	18.3 ±0.6		
	91	1282	10.0	2.59	0.918	5.82±1.66	2.74			29.5 ±0.9	22.5 ±0.9		
576	248	1101	28.6	7.40	1.049	0.64±0.47	0.55	0.77±0.79	0.86	2.83±0.24	1.61±0.24		
	215	1145	24.8	6.41	1.013	4.20±0.53	0.58			5.73±0.29	4.24±0.29		
	174	1198	20.0	5.19	0.977	12.0 ±0.7	0.8	11.9 ±1.2	1.3	14.8 ±0.4	12.7 ±0.4	2.08±0.25	−2.21±0.54
	131	1251	15.1	3.91	0.943	13.2 ±1.2	1.4			19.1 ±0.7	15.7 ±0.7		
	91	1299	10.5	2.72	0.918	6.18±2.20	3.15			27.8 ±1.2	21.2 ±1.2	12.7 ±0.8	−0.77±1.56
630	198	1201	24.9	6.46	0.984	8.19±0.83	0.94			11.2 ±0.5	9.80±0.50		

TABLE II. Hydrogen electroproduction cross sections, laboratory angle 135°. (All cross sections in units of 10^{-35} cm²/sr Mev.)

E_1	E_2	E	q^2 (10^4 Mev²)	q^2 (10^{26} cm^{-2})	ϵ	σ_{thick}	$\Delta\sigma_{\text{thick}}^{\max}$	σ_{thin}	$\Delta\sigma_{\text{thin}}^{\max}$	σ_{uncorr}	$\sigma_{\max}$	$\sigma_{\text{uncorr}}^{+}$	$\sigma_{\text{thick}}^{+}$
563	197	1091	37.9	9.81	1.032	0.83±0.21	0.23			1.19±0.11	0.82±0.11	1.21±0.23	−0.36±0.47
	156	1160	30.0	7.77	0.995	2.53±0.38	0.41			3.46±0.21	2.98±0.21	0.63±0.13	−0.19±0.27
	130	1202	25.0	6.47	0.976	5.79±0.32	0.45			7.70±0.20	7.11±0.20	1.67±0.23	−0.76±0.47
	103	1244	19.8	5.13	0.953	7.08±0.81	0.97			11.0 ±0.5	10.2 ±0.5		
	78	1281	15.0	3.88	0.937	4.00±1.09	1.51			13.8 ±0.6	12.6 ±0.6	6.95±0.59	−0.44±1.14
607	204	1102	42.3	10.95	1.024	0.66±0.16	0.17			0.97±0.09	0.65±0.09	1.82±0.19	−0.58±0.39
	169	1163	35.0	9.07	0.998	3.12±0.30	0.30			3.18±0.17	2.79±0.17	0.47±0.11	−0.25±0.23
	146	1202	30.3	7.84	0.976	4.50±0.26	0.32			5.70±0.15	5.24±0.15	1.28±0.19	0.06±0.37
	122	1240	25.3	6.54	0.961	5.23±0.42	0.66			7.80±0.25	7.21±0.25	2.22±0.27	0.37±0.53
	94	1284	19.5	5.05	0.947	3.50±0.74	1.53			9.62±0.40	8.78±0.40	4.30±0.43	−0.62±0.84
645	215	1102	47.3	12.26	1.025	0.25±0.24	0.25			0.79±0.12	0.53±0.12	1.80±0.25	−1.68±0.56
	182	1162	40.0	10.38	1.002	1.55±0.27	0.29			2.15±0.15	1.82±0.15		
	159	1201	35.0	9.07	0.983	3.76±0.27	0.30			4.53±0.15	4.14±0.15	1.10±0.19	−0.32±0.34
	139	1235	30.6	7.93	0.971	4.16±0.48	0.54			5.60±0.27	5.14±0.27		
	114	1275	25.1	6.50	0.957	3.03±0.59	0.74			6.61±0.32	5.91±0.32	2.10±0.38	−1.15±0.77
684	231	1092	53.9	13.97	1.028	0.01±0.20	0.21			0.43±0.10	0.21±0.10		
	192	1164	44.8	11.61	0.998	1.76±0.24	0.24			1.80±0.14	1.52±0.14		
	171	1202	39.9	10.34	0.987	2.48±0.22	0.24	2.08±0.37	0.41	3.18±0.12	2.86±0.12	0.98±0.16	0.16±0.31
	128	1275	29.9	7.74	0.961	2.92±0.49	0.56			4.89±0.27	4.42±0.27		
	107	1309	25.0	6.47	0.951	2.34±0.63	0.81			6.50±0.34	5.89±0.34		

model which yields the form

$$F(q^2)=\left(1+\frac{q^2(r_{nm})^2}{12}\right)^{-2}. \tag{19}$$

The neutron charge form factor was assumed to vanish, and the proton charge and magnetic moment radii were both taken to be 0.8 f, again using an exponential model.[4] The coupling constant f^2 is taken throughout as 0.09.[5] Other reasonable values of f^2 (e.g., 0.08 or 0.07) can shift the theoretical curves as much as 10%, with smaller values of f^2 leading to larger cross sections (at

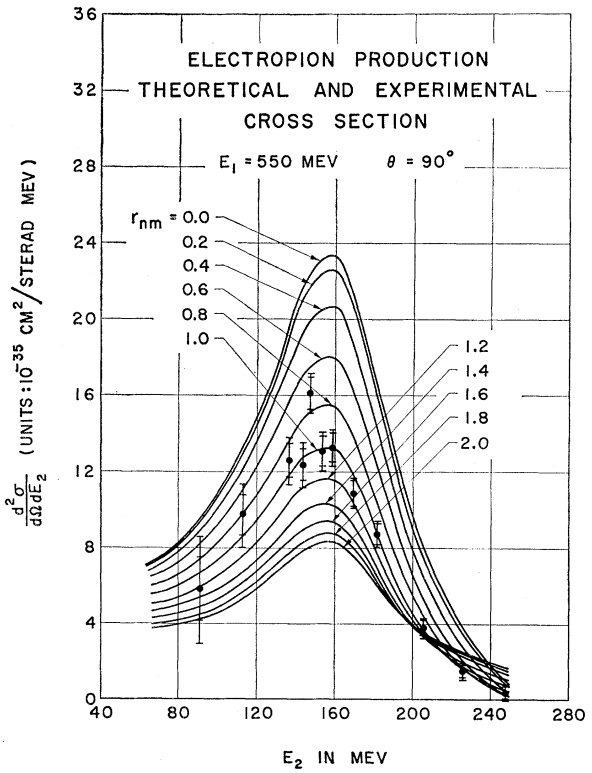

FIG. 4. Experimental and theoretical proton cross sections for $E_1=550$ Mev, $\theta=90°$. The theoretical curves given are those discussed in the text, evaluated for various values of r_{nm}, the neutron root mean square magnetic moment radius in units of the fermi (exponential model). The proton charge and moment distribution are assumed to be exponential with an rms radius of 0.8 f, and the neutron charge form factor is assumed identically zero. The experimental points are those derived from the "thick" radiator extrapolation. The outer error bars are derived from the assumption that the extrapolation factor ϵ may be in error by $\pm 5\%$; the inner error bars result from assuming the calculated values of ϵ are correct.

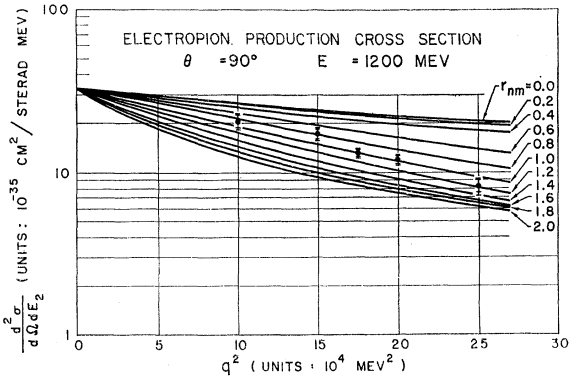

FIG. 5. Proton data obtained at laboratory angle 90° at constant center-of-mass energy $E=1200$ Mev (i.e., at "resonance"). The abscissa is the square of the 4-momentum transfer in units of 10^4 Mev^2. The neutron rms magnetic moment radius (in fermis) appropriate to each theoretical curve is indicated. Error bars are as in Fig. 4. Again the curves are based on an exponential model for both the proton and neutron, with the proton charge and moment radii 0.8 f, and the neutron charge form factor identically zero.

resonance). This dependence on f^2 is due almost entirely to the π^0 contribution, the π^+ contribution being relatively insensitive.

From Fig. 4, it may be seen that the data tend to peak at a lower final electron energy (higher center-of-mass energy) than predicted by theory. This appears to be the case at all the energies and angles investigated, although not enough data were obtained to determine how large this peak shift, if real, might be.

Figures 5 and 6 show the 90° and 135° resonance data ($E=1200$ Mev). It is seen that the data are most nearly in agreement with a neutron magnetic moment radius of 1.0 f. Since the theory is less reliable for larger values of q^2, the best measurements lie near the middle of the range of q^2 studied, where the various values of r_{nm} lead to experimentally distinguishable predictions while the theory is still expected to be reasonably accurate. However, the theory may be in error by 15% or more even in this range.

For ease of visualization, much of the data is presented isometrically in Fig. 7. A kinematic conversion factor, derived from the expressions given by Dalitz and Yennie,[2] has been applied to the 90° data to make it possible to present both 90° and 135° data on the same

TABLE III. Deuterium electroproduction cross sections, laboratory angle 90°. (All cross sections in units of 10^{-35} cm^2/sr Mev.)

E_1	E_2	E	q^2 (10^4 Mev^2)	q^2 (10^{26} cm^{-2})	ϵ	σ_{thick}	$\Delta\sigma_{\text{thick}}^{\max}$	σ_{thin}	$\Delta\sigma_{\text{thin}}^{\max}$	σ_{uncorr}	$\sigma_{\text{uncorr}}^{+}$	$\sigma_{\text{thick}}^{+}$
461	109	1201	10.0	2.60	0.986	28.2 ±2.2	3.1			48.1±1.2		
523	193	1140	20.2	5.19	1.053	9.47±1.35	2.18			27.7±0.7	9.50±0.70	0.94±1.44
	169	1170	17.7	4.56	1.033	21.0 ±1.3	1.5			25.6±0.7		
	146	1198	15.3	3.93	1.007	25.8 ±1.6	1.9	22.6±2.7	3.2	33.8±0.9	5.08±0.62	−3.10±1.32
	122	1228	12.8	3.23	0.987	26.4 ±2.0	2.7			43.4±1.1		
	96	1258	10.0	2.60	0.972	28.9 ±2.5	3.8			56.1±1.4	21.3 ±1.5	4.89±2.85
550	159	1200	17.5	4.52	1.016	23.2 ±1.1	1.3			28.2±0.6		
576	174	1198	20.0	5.19	1.025	18.8 ±1.1	1.3			23.9±0.6	3.61±0.42	−0.16±0.85
630	198	1201	24.9	6.43	1.031	17.2 ±1.3	1.9			30.7±0.7		

TABLE IV. Deuterium electroproduction cross sections, laboratory angle 135°. (All cross sections in units of 10^{-35} cm²/sr Mev.)

E_1	E_2	E	q^2 (10^4 Mev²)	q^2 (10^{26} cm^{-2})	ϵ	σ_{thick}	$\Delta\sigma_{thick}^{max}$	σ_{thin}	$\Delta\sigma_{thin}^{max}$	σ_{uncorr}	σ_{uncorr}^{+}	σ_{thick}^{+}
563	190	1103	36.5	9.46	1.073	1.76±0.46	0.58			4.53±0.23	1.38±1.12	−0.28±0.24
	156	1160	30.0	7.77	1.043	5.37±0.51	0.57			7.02±0.28	1.10±0.16	−0.36±0.34
	130	1202	25.0	6.47	1.022	8.32±0.42	0.70			11.8 ±0.3	3.12±0.29	−1.01±0.60
	103	1244	19.8	5.13	1.002	11.2 ±1.0	1.3			18.3 ±0.5		
	78	1281	15.0	3.88	0.985	11.0 ±1.4	2.1			25.7 ±0.8		
607	204	1102	42.3	10.95	1.072	2.98±0.64	0.78			6.37±0.33	2.26±0.20	0.30±0.42
	169	1163	35.0	9.07	1.046	3.71±0.38	0.44			5.19±0.20	0.94±0.14	−0.02±0.29
	146	1202	30.3	7.84	1.025	6.47±0.32	0.44	6.52±0.75	0.85	9.19±0.17	2.40±0.24	0.11±0.48
	122	1240	25.3	6.54	1.010	7.40±0.52	0.99			12.8 ±0.4	4.03±0.34	0.53±0.67
	94	1284	19.5	5.05	0.995	6.56±0.96	1.44			17.6 ±0.5	9.27±0.58	1.05±1.14
645	159	1201	35.0	9.07	1.031	5.86±0.38	0.44			7.52±0.20	1.72±0.19	0.40±0.37
684	171	1202	39.9	10.34	1.035	4.39±0.36	0.42			5.95±0.19	1.99±0.20	0.94±0.38

plot. Only those data which correspond kinematically to one of the theoretical curves shown are included.

VIII. DEUTERON DATA

The deuteron data are summarized in Tables III and IV. The notation is the same as was defined above for the proton tables. The values of q^2 and E given correspond to the two-body kinematics [Eqs. (3) and (4)].

The observed ratios of deuteron to proton cross sections at $E=1200$ Mev are plotted in Fig. 8. The solid curve is the result of folding the deuteron momentum distribution into the proton and neutron cross sections as calculated by Gartenhaus and Lindner, and taking the ratio with the theoretical proton cross section. The neutron rms magnetic moment radius was assumed to be 1.0 f for this calculation, while the proton charge and moment radii were again taken as 0.8 f. The agreement with such a simple model is seen to be poor.

A plot of the observed deuteron inelastic spectrum for the case $E_1=523$ Mev, $\theta=90°$ is given in Fig. 9. Again the solid curves are derived from a folding together of the deuteron momentum distribution and the free-proton and -neutron theoretical electropion production cross sections.

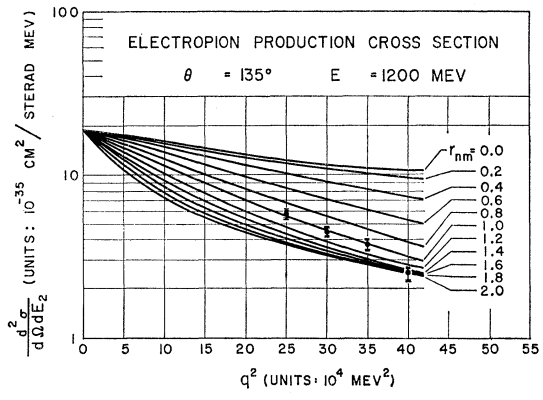

FIG. 6. Proton data obtained at laboratory angle 135°. Details are as in Fig. 5.

IX. CONCLUSIONS

The proton data seem most consistent with a root mean square neutron magnetic moment radius of 1.0 f. However, there still remain very considerable theoretical uncertainties, and the data[12–14] are therefore probably

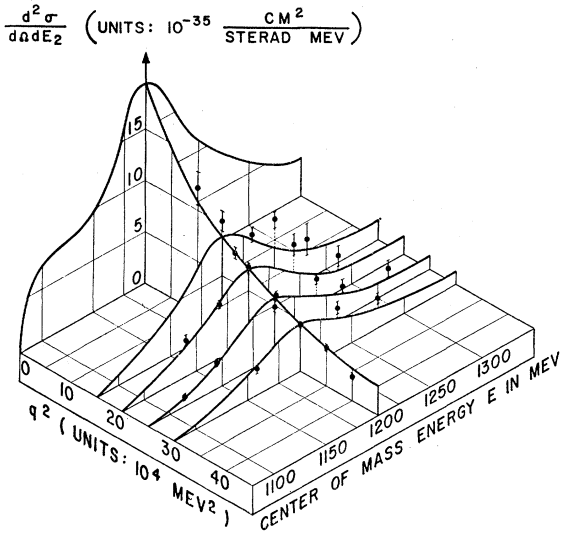

FIG. 7. Three-dimensional plot of some of the proton data versus the center-of-mass energy E and q^2, the square of the 4-momentum transfer. The solid curves are theoretical for $r_{nm}=1.0$ f, $\theta=135°$. Part of the data shown are 90° data which have been converted to 135° through multiplication by a purely kinematic factor which can be obtained from the theory of Dalitz and Yennie. In cases where it is not otherwise clear, the data points have been connected to the appropriate theoretical curve by a dashed line.

[12] M. R. Yearian and R. Hofstadter, Phys. Rev. **110**, 552 (1958).
[13] S. Sobottka, Phys. Rev. **118**, 831 (1960).
[14] H. W. Kendall, J. I. Friedman, and P. Gram, Bull. Am. Phys. Soc. **5**, 270 (1960).

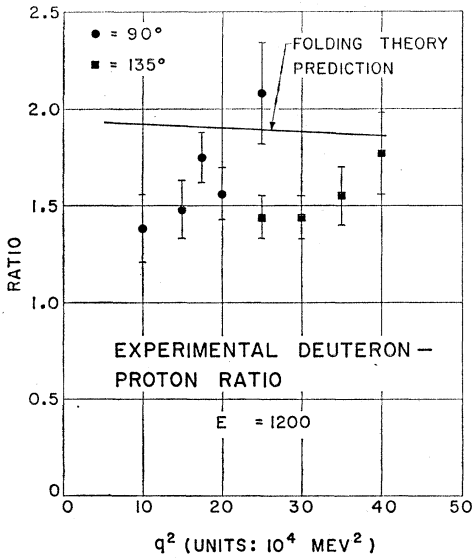

FIG. 8. Ratio of the experimental deuteron cross section to the experimental proton cross section. All points correspond to center-of-mass energy $E=1200$ Mev. The abscissa is the square of the invariant 4-momentum transfer q^2. The solid curve refers to the predicted ratio from a simple folding calculation, assuming $r_{nm}=1.0$ f.

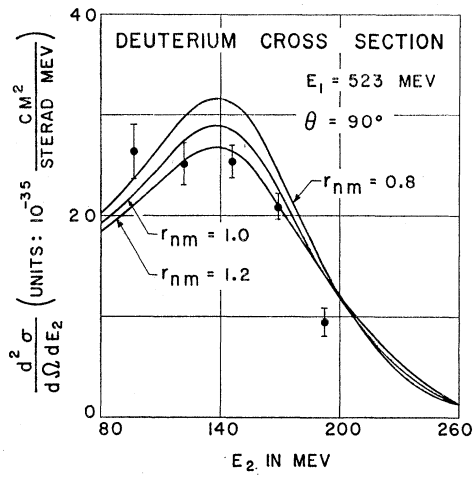

FIG. 9. Experimental spectrum of electrons which inelastically scatter from deuterium, with the production of pions, at $E_1=523$ Mev, $\theta=90°$. The solid curves are the predictions of a simple folding theory for the indicated values of the neutron rms magnetic moment r_{nm} in fermis.

consistent with the smaller neutron radii which are obtained by the deuteron methods.

The proton data appear to fit the shape of the predicted spectrum fairly well below the resonance. However, in every case the data are in generally poor agreement for the larger center-of-mass energies. This behavior points to a real disagreement with the present theory for center-of-mass energies above the resonance energy $E=1200$ Mev, and is not attributable to experimental error. However, the theory is expected to be less reliable for these large values of E as well as for the larger values of q^2.

The deuteron production cross section is considerably smaller than would be expected if the nucleons behaved as freely moving nucleons. The deuteron to proton cross-section ratio is constant within the experimental error for all the $E=1200$ Mev points, and has an average value of 1.6.

ACKNOWLEDGMENTS

It is a pleasure to thank Professor R. Hofstadter for proposing the experiment and for many helpful discussions concerning experimental problems, particularly during the earliest and most difficult phases of the work. I would also like to thank C. Lindner for clarification of several theoretical points, and for making some of his calculations available; L. Hand for his help with the problem of competing processes; A. Goldberg, Dr. J. Friedman, R. Alvarez, and E. Allton for helpful discussions; R. Alvarez, G. Burleson, P. Gram, L. Hand, N. Pearson, T. Sanders, and S. Sobottka for help with the tedious process of taking data; M. Ryneveld for his assistance in setting up for runs; C. Olson for his help with several electronic problems; and finally, the members of the machine operating crew, headed by R. Gilbert, for providing smooth operation of the linear accelerator through many nights of running.